Weierstraß-Institut

für Angewandte Analysis und Stochastik

Leibniz-Institut im Forschungsverbund Berlin e. V.

Numerical simulation of carrier transport in semiconductor devices at cryogenic temperatures

Markus Kantner, Thomas Koprucki

submitted: September 06, 2016

Weierstraß-Institut
Mohrenstr. 39
10117 Berlin
Germany
E-Mail: markus.kantner@wias-berlin.de
         thomas.koprucki@wias-berlin.de

Abstract

At cryogenic temperatures the electron-hole plasma in semiconductor materials becomes strongly degenerate, leading to very sharp internal layers, extreme depletion in intrinsic domains and strong nonlinear diffusion. As a result, the numerical simulation of the drift-diffusion system suffers from serious convergence issues using standard methods. We consider a one-dimensional p-i-n diode to illustrate these problems and present a simple temperature-embedding scheme to enable the numerical simulation at cryogenic temperatures. The method is suitable for forward-biased devices as they appear e.g. in optoelectronic applications.

1 Introduction

Electronic devices based on semiconductor technology can be employed on a huge temperature range – from several hundreds of Kelvin down to a few mK near the absolute zero. [3] Applications at cryogenic temperatures are manifold, e.g. space exploration missions require electronics capable of efficient and reliable operation at low temperatures. [9]. On the other hand, the availability of compact, commercial cryocoolers greatly supports the development of novel, easy-to-use light sources. These include in particular quantum-cascade lasers as THz radiation sources operating at 65 K [11] and single-photon emitters for quantum communication systems operating at around 4 to 30 K [12].

For the design of novel devices, numerical simulation of carrier transport has become an indispensable tool. However, accurate modeling as well as the implementation of robust simulation tools is challenging for applications far below room temperature. [13, 10]

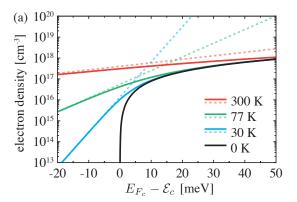# 2 Van Roosbroeck system and low temperature modeling aspects

The standard model to describe charge carrier transport in semiconductor devices is the isothermal *van Roosbroeck system*, which is also applicable at very low temperatures. [13, 10, 3] It describes the charge carrier transport in bipolar semiconductors in a self-consistent electric field. The equations are given as

$$-\nabla \cdot \varepsilon_0 \varepsilon_s \nabla \psi = qC + q \sum_{\alpha=\{c,v\}} z_\alpha u_\alpha, \tag{1}$$

$$q\partial_t u_\alpha + z_\alpha \nabla \cdot \mathbf{j}_\alpha = -qR, \qquad \alpha \in \{c, v\}, \tag{2}$$

$$\mathbf{j}_\alpha = -q\mu_\alpha u_\alpha \nabla \phi_\alpha \tag{3}$$

on $\Omega \subset \mathbb{R}^d$, $d = 1, 2, 3$. Here, ψ denotes the electric potential, ε_s is the relative permittivity, $C = N_D^+ - N_A^-$ is the net doping profile, $u_c = n$ denotes the density of electrons in the
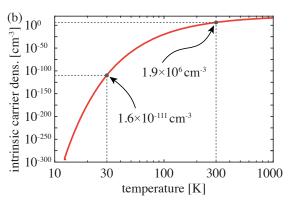
Figure 1: (a) Electron density as a function of the electron Fermi level for several temperatures. Fermi-Dirac statistics are indicated by solid curves, the Maxwell-Boltzmann approximations are shown as dashed lines. The fully degenerate limit ($T = 0\,\mathrm{K}$) is plotted for comparison. (b) Temperature dependence of the intrinsic carrier density in GaAs.

conduction band and $u_v = p$ are the holes in the valence band. The different signs of charge are reflected by the charge numbers $z_v = +1$ and $z_c = -1$. The carrier densities obey Fermi-Dirac statistics and are given as

$$u_\alpha = N_\alpha F_{1/2}\left(\eta_\alpha\right), \quad N_\alpha = 2\left(\frac{2\pi m_\alpha^* k_B T}{h^2}\right)^{3/2}, \quad \eta_\alpha = z_\alpha \frac{\mathcal{E}_\alpha - E_{F_\alpha}}{k_B T}, \tag{4}$$

with the effective density of states N_α, the Fermi energy level $E_{F_\alpha} = -q\phi_\alpha$ and $\mathcal{E}_\alpha = E_\alpha - q\psi$. Here m_α^* denotes the effective mass, E_α is the band edge energy, ϕ_α represents the quasi-Fermi potential, T is the lattice temperature and F_ν is the Fermi-Dirac integral of order ν. The continuity equations (2) describe the carrier transport and recombination dynamics. Eq. (3) defines the current density vector $\mathbf{j}_\alpha$, which is proportional to a mobility μ_α and the gradient of the quasi-Fermi potential. The net recombination rate R comprises various recombination mechanisms. The fundamental constants occurring are the vacuum permittivity ε_0, Boltzmann's constant k_B, Planck's constant h and the elementary charge q. The system (1)-(3) is subject to mixed Dirichlet-Neumann boundary conditions modeling electrical contacts and artificial boundaries, see e.g. [4].

Most of the material parameters show a strong temperature dependence. At room temperature, thermally excited phonons (lattice vibrations) provide the dominant scattering channels for the freely roaming carriers, leading to mobility reduction and increased non-radiative recombination. At very low temperatures, however, phonons are strongly suppressed, resulting in different recombination kinetics and carrier mobilities that typically are limited by ionized impurity scattering. Moreover, due to the lack of sufficient thermal excitation, the built-in dopants tend to *freeze out* at low temperatures. This leads to incomplete ionization effects, which need to be included appropriately, see e.g. [13, 1]. On the other hand, in the case of heavy doping beyond a critical value, the metal-insulator transition leads to complete ionization (e.g. $N_D^+ \approx N_D$) even at extremely low temperatures. [8]
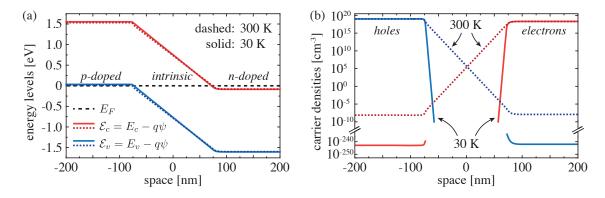
2

Figure 2: Comparison of the thermal equilibrium in a 1D p-i-n diode for 30 K and 300 K. Even though (a) the built-in potential and energy bands differ only slightly, (b) the carrier densities vary drastically when passing to the cryogenic case. We assume a piecewise constant doping profile, complete ionization ($N_D^+ = 2 \times 10^{18}$ cm^{-3}, $N_A^- = 1 \times 10^{19}$ cm^{-3}) and the parameters $E_c = 1.52$ eV, $E_v = 0$ eV, $m_c^* = 0.067 m_e$, $m_v^* = 0.5 m_e$ (m_e is the free electron mass).

3   Degeneracy effects at cryogenic temperatures

At room temperature and for moderate carrier densities ($\eta \lesssim -1$), it is common to simplify Eq. (4) by an exponential $F_{1/2}(\eta) \approx e^\eta$ (Maxwell-Boltzmann approximation). However, for low temperatures this approximation leads to fatal overestimation of carrier densities as soon as the Fermi energy exceeds the band edge energy. This is illustrated in Fig. 1(a), which shows the electron density as a function of the difference between the Fermi energy and the conduction band edge. Of course, this overestimation propagates to all density-dependent quantities such as the currents and recombination rates. Furthermore, Fig. 1(a) indicates that at very low temperatures the carrier density becomes highly sensitive to small changes of the Fermi level. In the cryogenic limit Sommerfeld's expansion yields

$$\lim_{T \to 0\,\text{K}} u_\alpha = \frac{\pi}{3} \left(\frac{8 m_\alpha^*}{h^2} \right)^{3/2} \times \begin{cases} \left(z_\alpha \left[\mathcal{E}_\alpha - E_{F_\alpha} \right] \right)^{3/2} & \text{for } z_\alpha \left(\mathcal{E}_\alpha - E_{F_\alpha} \right) > 0, \\ 0 & \text{else.} \end{cases} \tag{5}$$

Obviously, the carrier statistics in the cryogenic limit coincides with the *fully degenerate limit* $F_{1/2}(\eta) \approx \frac{4}{3\sqrt{\pi}} \eta^{3/2}$ for $\eta \gg 1$, which usually applies for very high carrier densities. According to Eq. (5), for $T \to 0$ K the exponential low-density tail vanishes to identical zero, leading to full depletion wherever the Fermi energy drops below the band edge. The mathematical analysis of the van Roosbroeck system with carrier statistics as in Eq. (5) has been carried out in [6].

In order to illustrate the impact of the temperature on the carrier distribution, we consider a one-dimensional (1D) p-i-n diode at 30 K and 300 K, see Fig. 2. In the thermal equilibrium (zero bias), the carrier densities range over many orders of magnitude and the minority carrier densities tend to become extremely small (scaling as $u_{\text{minor}} \approx n_i^2 / u_{\text{major}}$). For comparison: The typical 300 K value $u_{\text{minor}} \sim 10^{-8}$ cm^{-3} drops down to around $u_{\text{minor}} \sim 10^{-240}$ cm^{-3} at 30 K. This is mainly caused by the strong temperature-dependence of the intrinsic carrier density n_i (cf. Fig. 1(b)) and leads to the formation of extremely sharp layers between the intrinsic and doped regions (cf. Fig. 2(b)). In order to focus on the temperature-induced degeneracy effects, we only consider
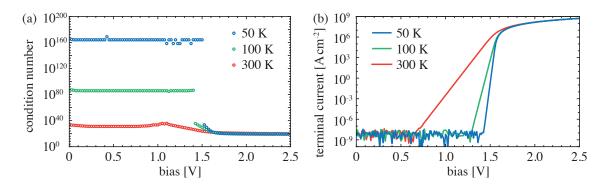
Figure 3: (a) Condition number estimate of the Jacobian for the p-i-n diode problem (cf. Fig. 2) at different temperatures and (b) current-voltage curves. The sudden drop of the condition number roughly coincides with the threshold voltage. We assume stationary Shockley-Read-Hall (SRH) recombination as described e.g. in [4]. Besides the parameters listed in the caption of Fig. 2, we assume the mobilities $\mu_c = 20000\,\mathrm{cm^2V^{-1}s^{-1}}$, $\mu_v = 300\,\mathrm{cm^2V^{-1}s^{-1}}$ and SRH lifetimes $\tau_c = 70\,\mathrm{\mu s}$, $\tau_v = 200\,\mathrm{\mu s}$.

the explicit temperature-dependence in Eq. (4), whereas all other parameters are kept constant throughout this paper.

Finally, the degeneracy of carrier statistics also has a significant impact on the diffusive currents. One can rewrite Eq. (3) in the drift-diffusion form as $\mathbf{j}_\alpha = -q\mu_\alpha u_\alpha \nabla \psi - z_\alpha q D_\alpha \nabla u_\alpha$, where the diffusion coefficient obeys the generalized Einstein-relation $D_\alpha = k_B T g(\eta_\alpha)/q$ with the nonlinear diffusion factor

$$g(\eta_\alpha) = F_{1/2}(\eta_\alpha)/F_{-1/2}(\eta_\alpha).\tag{6}$$

Fig. 4(b) shows, that this factor can be particularly large at low temperatures.

4 Numerical approximation and low temperature convergence issues

We aim for a discretization of the system Eq. (1)-(3) using a Voronoï box based finite volumes method in space and an implicit discretization in time, see e.g. [4]. Moreover, we use a modified Scharfetter-Gummel scheme according to [2] and [7], taking the nonlinear diffusion factor Eq. (6) explicitly into account. Typically, for a bias sweep, one first solves the thermal equilibrium problem and then computes the biased configurations by successively changing the boundary conditions. In this numerical continuation procedure for each new step the previously computed solution can be used as an initialization. The discretized system is solved using a Newton iteration, taking the potentials $\{\psi, \phi_\alpha\}$ as basic variables.

For cryogenic temperatures this algorithm leads to serious convergence issues already close to the thermal equilibrium. The extremely small minority carrier densities (cf. Fig. 2(b)) dramatically impact the Jacobian, which becomes practically singular to finite precision arithmetics. As an indicator for the ill-posedness of the problem, we estimate the condition number κ of the Jacobian according to [5]. Fig. 4(a) clearly shows the tremendous increase of κ for decreasing tempera-
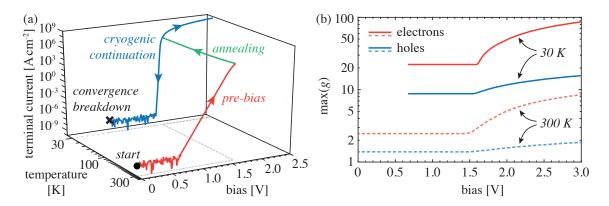
Figure 4: Numerical simulation of stationary drift-diffusion transport in the p-i-n diode at 30 K. (a) Continuation scheme for cryogenic simulations. After reaching flat band conditions, a solution at the cryogenic target temperature is obtained by an annealing phase. The approach facilitates e.g. the calculation of cryogenic current-voltage curves as shown in the plot. (b) At 30 K the maximum nonlinear diffusion factor Eq. (6) is about ten times larger than at 300 K.

ture. For large κ, the solution of the linear system becomes highly sensitive to round-off errors and cancellation effects, obstructing a reliable Newton update. As a consequence, the standard numerical continuation procedure starting at the thermal equilibrium can not be applied straightforwardly. To tackle this problem, in [10] the usage of extended-precision arithmetics has been suggested.

5   Two-step temperature-embedding scheme

In order to motivate an alternative continuation approach, we extend our considerations on the condition number and study its dependence on the applied bias for different temperatures. Interestingly, for bias values beyond the threshold (*flat bands*), the extremely high condition numbers of the cryogenic problems suddenly drop to a moderate order of magnitude, see Fig. 3. We attribute this behavior to the reduction of the extreme depletion of the minorities. This implies, that above the threshold the simulations can be carried out with standard methods.

For many applications, in particular in optoelectronics, one is mainly interested in the device behavior close to or beyond the flat band case. Inspired by the preceding observations, we propose a two-step temperature-embedding scheme, which is illustrated in Fig. 4(a). First, at a moderate temperature a bias sweep from the thermal equilibrium to a target voltage beyond the expected threshold is performed. In a second step, the temperature is successively decreased until reaching the cryogenic operation point. Starting from the attained cryogenic flat band solution, the actual computations of interest (e.g. voltage sweeps, small/large signal analysis) can be carried out. This approach is particularly suitable for transient simulations, since finite recombination lifetimes and mobilities counteract the rapid depletion below the threshold voltage. Please note that during the annealing phase (2nd step), all temperature-dependent material parameters need to be updated iteratively (or should be set to the cryogenic values in the very beginning). Moreover, it is essential to update the temperature-dependent boundary values at

5

the Ohmic contacts (built-in potential) in each temperature step.

For the parameters used, our approach works well down to 27 K using double precision – also for higher dimensional device geometries (2D, 3D). We observed quadratic convergence of Newton's method in each iteration step.

6 Conclusions

Near to the thermal equilibrium, the discretized van Roosbroeck system becomes ill-conditioned at cryogenic temperatures. We presented a temperature-embedding scheme, to circumvent the computationally troublesome regions. We have successfully demonstrated this approach for a p-i-n diode at $T = 30$ K. As an alternative, extended-precision arithmetics might be used for low temperature simulations. [10] However, this approach is computationally expensive.

The method proposed in this paper does not require any non-standard iteration schemes or precision demands and can be implemented without much effort.

References

[1] Akturk, A., Allnutt, J., Dilli, Z., Goldsman, N., Peckerar, M.: Device modeling at cryogenic temperatures: Effects of incomplete ionization. IEEE T. Electron Dev. **54**(11), 2984–2990 (2007).

[2] Bessemoulin-Chatard, M.: A finite volume scheme for convection–diffusion equations with nonlinear diffusion derived from the Scharfetter–Gummel scheme. Numer. Math. **121**, 637–670 (2012)

[3] Cressler, J.D., Mantooth, H.A.: Extreme Environment Electronics. CRC Press (2012)

[4] Farrell, P., Rotundo, N., Doan, D.H., Kantner, M., Fuhrmann, J., Koprucki, T.: Numerical Methods for Drift-Diffusion Models. In: Handbook of Optoelectronic Device Modeling and Simulation. Editor: Piprek, J., Taylor & Francis (2017, to appear)

[5] Hager, W. W.: Condition Estimates. SIAM J. Sci. Stat. Comp. **5**, 311–316 (1984).

[6] Jüngel, A.: Qualitative behaviour of solutions of a degenerate nonlinear drift-diffusion model for semiconductors. Math. Mod. Meth. Appl. S. **5**(4), 497–518 (1995).

[7] Koprucki, T., Rotundo, N., Farrell, P., Doan, D.H., Fuhrmann, J.: On thermodynamic consistency of a Scharfetter–Gummel scheme based on a modified thermal voltage for drift-diffusion equations with diffusion enhancement. Opt. Quant. Electron. **47**(6), 1327–1332 (2015).

[8] Mott, N.F.: Metal-insulator transitions. Taylor & Francis, London (1974).

[9] Patterson, R.L., Hammoud A., Elbuluk, M.: Assessment of electronics for cryogenic space exploration missions. Cryogenics **46**, 231–236 (2006).

[10] Richey, D.M., Cressler, J.D., Jaeger, R.C.: Numerical simulation of SiGe HBT's at cryogenic temperatures. J. Phys. IV France **04**(C6), C6–127–C6–32 (1994).

[11] Richter, H., Greiner-Bär, M., Pavlov, S.G., Semenov, A.D., Wienold, M., Schrottke, L., Giehler, M., Hey, R., Grahn, H.T., Hübers, H.-W.: A compact, continuous-wave terahertz source based on a quantum-cascade laser and a miniature cryocooler. Opt. Express **18**(10), 10179 (2010).

[12] Schlehahn, A., Thoma, A., Munnelly, P., Kamp, M., Höfling, S., Heindel, T., Schneider, C., Reitzenstein, S.: An electrically driven cavity-enhanced source of indistinguishable photons with 61% overall efficiency. APL Photonics **1**, 011301 (2016).

[13] Selberherr, S.: Low temperature MOS device modeling. In: Proc. of the 172nd Meeting of the Electrochem. Soc., vol. 88-9, pp. 70–86. Honolulu (1987)